Analysis of optical interferometric measurements of guided acoustic waves in transparent solid media

X. Jia, Ch. Matteï, and G. Quentin

Citation: Journal of Applied Physics **77**, 5528 (1995); doi: 10.1063/1.359592
View online: http://dx.doi.org/10.1063/1.359592
View Table of Contents: http://scitation.aip.org/content/aip/journal/jap/77/11?ver=pdfcov
Published by the AIP Publishing

Analysis of optical interferometric measurements of guided acoustic waves in transparent solid media

X. Jia,[a] Ch. Matteï, and G. Quentin
Groupe de Physique des Solides, Universités Paris 7 et Paris 6, Unité Associée au CNRS No. 17, Tour 23, 2 place Jussieu, 75251 Paris Cedex 05, France

(Received 20 May 1994; accepted for publication 4 February 1995)

Guided acoustic waves propagating in transparent and isotropic solids are studied by optical interferometry via the photoelastic effect. Unlike the photoelastic technique, the interferometric method permits the measurement of the phase shift rather than the polarization change of the light passing through an acoustic field. By analyzing the acoustically induced change in the index ellipsoid of refraction, it is demonstrated that the optical phase shift is proportional to the *dilatation* or the relative change in volume of the material. The dilatation fields of the symmetric and antisymmetric Lamb modes S_0 and A_0, as well as that of the Rayleigh wave, were calculated. Experiments performed in fused quartz by the interferometric method are in good agreement with theoretical predictions. Compared to the conventional photoelastic technique, the interferometric measurement of acoustic wave is phase sensitive and quantitative. © *1995 American Institute of Physics.*

I. INTRODUCTION

Since the first experiments made by Lucas and Biquard[1] in France and Debye and Sears[2] in the U.S.A., acousto-optic effects have found wide interests for applications such as acousto-optic devices for light beam deflection, modulation, and signal processing.[3–5] In addition, the acousto-optic interaction affords a convenient way of optically probing the acoustic field inside a transparent medium. Unlike acoustic transducers, the optical detection does not disturb the acoustic fields under investigation. Many applications have been found in medical diagnosis and nondestructive evaluation.[4,6–8]

Acousto-optic modulation of the light traveling through an acoustic beam arises from refractive index variations associated with the strain fluctuations due to the acoustic waves. Since the acoustic wave interacts with the optical wave along the whole light path, optical techniques based on the acousto-optic interaction are usually limited to probing two-dimensional (2D) acoustic fields uniform along the propagation direction of the light. Among various optical techniques, two types are basically distinguished: optical diffraction and beam deflection. The first is referred to situations in which the optical beam is much wider than the acoustic wavelength. The acoustic wave acts as a moving phase grating, diffracting the light into different orders in the far optical field (Raman–Nath diffraction).[9] Schlieren visualization derived from this mechanism has extensively been used to study the propagation of acoustic waves in fluids.[10,11] The second method deals with the deflection of the light beam caused by the gradient of refractive index (mirage effect) when acoustic waves propagate in the medium.[12,13] Contrary to the preceding situation, the light beam is narrower than the acoustic wavelength here. Optical deflection techniques have also been widely used in photoacoustic and photothermal measurements in fluids.[14]

In solids the acousto-optic interaction becomes more complex than in fluids because the propagation of acoustic waves can additionally induce the optical birefringence. Generally speaking, the transmitted light exhibits both phase and polarization changes. The usual method, referred to as the photoelastic technique, is based on measurements of the polarization change of the light.[7] Like the Schlieren visualization the conventional photoelastic technique is sensitive only to acoustic intensities. Recently, we proposed an optical interferometric method for measuring bulk acoustic waves both in fluids and solids.[15,16] Unlike the usual displacement or velocity measurements at the vibrating surfaces,[17,18] the optical interferometry was arranged to measure acoustic pressures or strains inside transparent media. Different from the photoelastic technique, the interferometric method permits a quantitative measurement of the additional phase shift of the light induced by acoustic waves. The main advantage lies in its sensitivity to not only the magnitude but also the phase of acoustic signals.

In this paper, we present an extension of this interferometric method to the study of guided surface acoustic waves such as Lamb, Rayleigh, and Stoneley waves propagating in an isotropic solid. It is well known that these surface waves are of major importance in material characterization and acoustoelectric processing.[19–21] However, because of the anisotropic nature of the acousto-optic effect and the combined mechanical motions of the longitudinal and shear waves, the interaction of an optical wave with a surface acoustic wave is much more complicated than that with a bulk wave.[22–24] In Sec. II we will first analyze this problem, starting from the refractive index ellipsoid. The principles of the photoelastic and interferometric methods are illustrated using Jones formalism. The theoretical strain fields of the Lamb modes S_0 and A_0 as well as those of the Rayleigh wave are given in Sec. III. We then compare these results with the experimental data in Sec. IV.

[a]Electronic mail: jia@gps.jussieu.fr

 0021-8979/95/77(11)/5528/10/$6.00

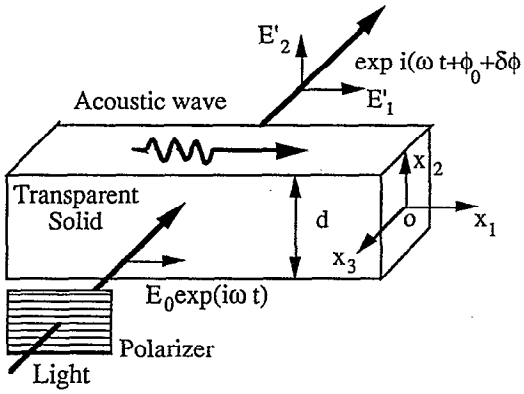

FIG. 1. Schematic diagram of the interaction between a light wave and a guided acoustic wave.

II. ANALYSIS OF THE ACOUSTO-OPTIC INTERACTION WITH SURFACE ACOUSTIC WAVES

A. Photoelastic effect

The interaction of the light with a guided acoustic wave is schematically illustrated in Fig. 1. The transparent solid is at rest optically isotropic. Without loss of generality the propagation direction of the acoustic wave can be taken as the x_1 axis, thus defining the plane x_1x_2 as the sagittal plane. The light travels in the direction x_3 perpendicular to the propagation direction of the acoustic wave. Because of the acoustic perturbations the solid medium becomes optically anisotropic. The resulting changes in the components of the dielectric tensor are[3–5]

$$\Delta\epsilon_{ij}=\Delta(1/n^2)_{ij}=-\epsilon^2 p_{ijkl}S_{kl}, \tag{1}$$

where ϵ is the dielectric constant of the isotropic solid and p_{ijkl} $(i,j,k,l=1,2,3)$ is the photoelastic tensor. The strain tensor S_{kl} is symmetric, and related to the particle displacement u_k by

$$S_{kl}=\frac{1}{2}\left(\frac{\partial u_k}{\partial x_l}+\frac{\partial u_l}{\partial x_k}\right). \tag{2}$$

Here the diagonal components S_{11}, S_{22}, and S_{33} are the longitudinal strains corresponding to the extension of a cube along the axes x_1, x_2, and x_3, whereas the off-diagonal components are associated with shear strains that do not contribute to volume change. In the present analysis, we consider only a "plane" guided acoustic wave, defined as a wave where no dependence of particle displacement on the direction x_2 perpendicular to the propagation direction x_1 is observed, i.e., a usual 2D acousto-optic configuration. In an isotropic guide there exist, in general, two independent acoustic wave solutions.[19,20] One is the Rayleigh type of wave with displacement components only in the sagittal plane (u_1 and $u_2\neq 0$), as is the case for Rayleigh, Lamb, and Stoneley waves. The second is the *SH* type of wave exhibiting transversely polarized displacements perpendicular to the sagittal plane (only $u_3\neq 0$), such as *SH* bulk waves and Love waves. The *SH* type of waves will not be considered in this work, because there is no acousto-optic effect on the light traveling along the direction parallel to the polarization of acoustic displacements.[3,16]

We are primarily concerned with the Rayleigh type of wave. According to Eq. (2), the associated strain tensor S_{kl} has three nonzero components: S_{11}, S_{22}, and S_{12}. Using the standard reduced notation,[11,20] the strain tensor can be written in the form of a column matrix S_m $(n=1,2,...,6)$ in which $S_1=S_{11}$, $S_2=S_{22}$, and $S_6=2S_{12}$. Substituting the strain components into Eq. (1), the variations of the dielectric tensor $\Delta\epsilon_{ij}$ in Eq. (1) can be expressed by a symmetric matrix in reduced notation:

$$(\Delta\epsilon)=\begin{pmatrix}\Delta\epsilon_1 & \Delta\epsilon_6 & 0\\ \Delta\epsilon_6 & \Delta\epsilon_2 & 0\\ 0 & 0 & \Delta\epsilon_3\end{pmatrix}, \tag{3}$$

with

$$\Delta\epsilon_1=-\epsilon^2(p_{11}S_1+p_{12}S_2),$$

$$\Delta\epsilon_2=-\epsilon^2(p_{12}S_1+p_{11}S_2),$$

$$\Delta\epsilon_3=-\epsilon^2 p_{12}(S_1+S_2),$$

$$\Delta\epsilon_6=-\epsilon^2(p_{11}-p_{12})S_6.$$

Here p_{mn} is a 6×6 photoelastic tensor written in terms of reduced subscripts. It may be noted that the acoustic strains transform the initial refractive index sphere into an ellipsoid, having its principal axes x,y no longer parallel to the geometrical axes x_1,x_2, due to the off-diagonal component $\Delta\epsilon_6$. The presence of $\Delta\epsilon_6$ is generally associated with the Rayleigh type of wave because $p_{11}\neq p_{12}$ in solid media.[3–5] Under these circumstances, the isotropic solid becomes optically biaxial. Polarized light passing through such a medium undergoes a phase shift and also a polarization rotation.

By diagonalizing the refractive index matrix in Eq. (3), its eigenvalues can be found, leading to the refractive index for eigenmode propagation.[5] With respect to the principal coordinates xyz, the ellipsoid equation may be written in a simple form

$$\frac{x^2}{n_x^2}+\frac{y^2}{n_y^2}+\frac{z^2}{n_z^2}=1, \tag{4}$$

with the major axes parallel to the principal directions x, y, and z. The respective lengths of these axes are $2n_x$, $2n_y$, and $2n_z$. In the approximation of weak perturbation $(\Delta n\ll n)$, the new principal refractive indices, defined as $n_{x,y,z}=\sqrt{1/\epsilon_{x,y,z}}$, are

$$n_x\approx n-(n^3/2)\left[\frac{(p_{11}+p_{12})}{2}(S_1+S_2)+\frac{(p_{11}-p_{12})}{2}\sqrt{(S_1-S_2)^2+4S_6^2}\right], \tag{5}$$

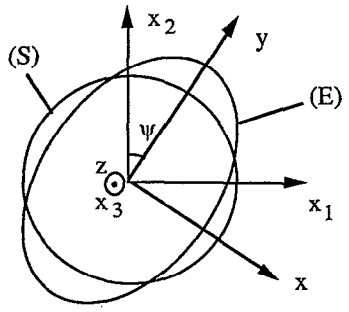

FIG. 2. The index sphere (S) of an isotropic solid becomes an ellipsoid (E) in the presence of acoustic strains.

$$n_y \approx n-(n^3/2)\left[\frac{(p_{11}+p_{12})}{2}(S_1+S_2)\right.$$
$$\left.-\frac{(p_{11}-p_{12})}{2}\sqrt{(S_1-S_2)^2+4S_6^2}\right],$$
$$n_z \approx n-(n^3/4)p_{12}(S_1+S_2).$$

The new principal axes xyz are obtained by rotating the geometrical axes x_1, x_2 around the x_3 axis by angle ψ, as illustrated in Fig. 2:

$$\psi=\arctan\left(\frac{2S_6}{(S_1-S_2)+\sqrt{(S_1-S_2)^2+4S_6^2}}\right). \tag{6}$$

For the simple example of longitudinal motion along the direction x_1, the only nonzero strain component is defined by $S_1=\partial u/\partial x_1$ [Eq. (2)]. In this case, we have

$$\Delta n_x=-(1/2)n^3p_{11}S_1,$$
$$\Delta n_y=\Delta n_z=-(1/2)n^3p_{12}S_1,$$
$$\psi=0,$$

which implies that the solid becomes uniaxial with the new principal axes still parallel to the geometrical axes. On the other hand, a plane shear wave, in which the particle displacement is only in the direction x_2 (SV shear wave), is defined by the relations $S_1=S_2=0$, $S_6=\partial u_2/\partial x_1$, yielding

$$\Delta n_x=-\Delta n_y=-(1/2)n^3(p_{11}-p_{12})S_6,$$
$$\Delta n_z=0, \quad \text{and} \quad \psi=45°.$$

The new principal axes are now rotated by 45° around the x_3 axis.[16]

B. Photoelastic and interferometric measurements of surface acoustic waves

It is seen in the preceding discussion that the propagation of a guided acoustic wave transforms, in general, the solid into an optically biaxial medium. Consider now a light beam traveling in this solid along the direction $-x_3$ (Fig. 1). The electric field $\mathbf{E}$ of the incident light is expressed, using the Jones formulation, in matrix form, by

$$\mathbf{E}=\begin{pmatrix}E_1\\E_2\end{pmatrix}e^{i(\omega t-kx_3)}. \tag{7}$$

For simplicity in the analysis, the propagation term $\exp i(\omega t-kx_3)$ will be neglected in the following discussion. To determine how the light propagates in an optically birefringent medium, it is useful to decompose the light into a linear combination of two eigenmodes in which the electric fields are parallel to the principal axes x,y. This can done by the coordinate transformation

$$\begin{pmatrix}E_x\\E_y\end{pmatrix}=\begin{pmatrix}\cos\psi & \sin\psi\\-\sin\psi & \cos\psi\end{pmatrix}\begin{pmatrix}E_1\\E_2\end{pmatrix}\equiv R(\psi)\begin{pmatrix}E_1\\E_2\end{pmatrix}. \tag{8}$$

Here $R(\psi)$ is the rotation matrix which allows the matrix representation of the $\mathbf{E}$ fields to be transformed from the geometrical axes to the principal ones. Let n_x and n_y be the refractive indices of the eigenmodes $\mathbf{E}_1$ (E_x, 0) and $\mathbf{E}_2$ (0, E_y), respectively. The polarization state of the light $\mathbf{E}'$ emerging from the acoustic beam is written in the principal coordinates x,y as follows:

$$\begin{pmatrix}E_x'\\E_y'\end{pmatrix}=\begin{pmatrix}\exp(-in_x\omega l/c) & 0\\0 & \exp(-in_y\omega l/c)\end{pmatrix}\begin{pmatrix}E_x\\E_y\end{pmatrix}, \tag{9}$$

where l is the thickness along the x_3 direction of the acoustic beam inside the solid and ω the frequency of light. As the light propagates in the crystal, the polarization state of the emerging light is changed[5] because of the difference in phase shift between the "slow mode" $\mathbf{E}_1$ and the "fast mode" $\mathbf{E}_2$.

Introducing two parameters Γ and ϕ, defined as

$$\Gamma=(n_x-n_y)\frac{\omega l}{c} \tag{10}$$

and

$$\phi=\frac{1}{2}(n_x+n_y)\frac{\omega l}{c}, \tag{11}$$

the emerging light given in Eq. (9) is rewritten in terms of Γ and ϕ:

$$\begin{pmatrix}E_x'\\E_y'\end{pmatrix}=e^{-i\phi}\begin{pmatrix}\exp(-i\Gamma/2) & 0\\0 & \exp(i\Gamma/2)\end{pmatrix}\begin{pmatrix}E_x\\E_y\end{pmatrix}$$
$$\equiv W\begin{pmatrix}E_x\\E_y\end{pmatrix}. \tag{12}$$

It can be noticed that Γ is the phase retardation measuring the relative phase change between the eigenmodes, that is, the optical birefringence induced by acoustic waves, and ϕ is the mean absolute phase shift of the light transmitted through the medium. The expression for the emerging light $\mathbf{E}'$ in geometrical coordinates x_1,x_2 can be obtained by transforming back from the principal coordinates x,y. Combining Eqs. (8), (9), and (12) the emerging light is related to the incident one as follows:

$$\begin{pmatrix}E_1'\\E_2'\end{pmatrix}=R(-\psi)\begin{pmatrix}E_x'\\E_y'\end{pmatrix}\equiv W_0\begin{pmatrix}E_1\\E_2\end{pmatrix}, \tag{13}$$

where $W_0=R(-\psi)WR(\psi)$ is

$$W_0 = e^{-i\phi}\begin{pmatrix} \cos(\Gamma/2) - i\,\sin(\Gamma/2)\cos 2\psi & -i\,\sin(\Gamma/2)\sin 2\psi \\ -i\,\sin(\Gamma/2)\sin 2\psi & \cos(\Gamma/2) + i\,\sin(\Gamma/2)\cos 2\psi \end{pmatrix}. \tag{14}$$

Consequently, the propagation of the light across the medium is entirely characterized by the Jones matrix W_0.

If the incident light is initially polarized in the x_1 direction with the help of a polarizer, as shown in Fig. 1,

$$\mathbf{E} = E_0\begin{pmatrix} 1 \\ 0 \end{pmatrix}, \tag{15}$$

the emerging light at the output is obtained from Eq. (13):

$$\begin{aligned} \mathbf{E}' &= W_0 E_0\begin{pmatrix} 1 \\ 0 \end{pmatrix} \\ &= E_0 e^{-i\phi}\begin{pmatrix} \cos(\Gamma/2) - i\,\sin(\Gamma/2)\cos 2\psi \\ -i\,\sin(\Gamma/2)\sin 2\psi \end{pmatrix} \\ &\approx E_0 e^{-i\phi}\begin{pmatrix} 1 \\ -i(\Gamma/2)\sin 2\psi \end{pmatrix}. \end{aligned} \tag{16}$$

The approximation on the right-hand side of the above equation is valid for low intensity acoustic waves. In conventional photoelastic measurements, the transmission intensity of the light is measured. The phase factor $\exp(-i\phi)$ in Eq. (16) is not observable and usually neglected. If an analyzer placed at the output of the system is crossed with respect to the polarizer at the input, the component of $\mathbf{E}'$ in the direction x_2 is selected. Putting Eqs. (5) and (10) into Eq. (16), we obtain the transmission intensity I:

$$I \propto \Gamma^2 \propto (S_1 - S_2)^2 + 4S_6^2, \tag{17}$$

proportional to the square of acoustic strain. This is the basic principle of the photoelastic technique.[7] According to Eqs. (16) and (17), the light intensity diffracted by acoustic waves into the direction x_2 is much smaller than that of the incident light $\mathbf{E}$ polarized in the direction x_1. Moreover, it is seen from Eq. (17) that the acoustic strains or stresses measured with the photoelastic method are rather complicated, being neither pure longitudinal nor pure shear.

We describe now the principle of our interferometric method, based upon the measurement of the phase shift ϕ in Eq. (16). Substituting Eq. (5) into Eq. (11), the mean optical phase shift ϕ is written as

$$\phi = \phi_0 + \delta\phi \equiv \phi_0 - n^3 \frac{\omega l}{2c}(p_{11} + p_{12})(S_1 + S_2). \tag{18}$$

Here $\phi_0 = n\omega l/c$ is a constant phase shift due to the finite thickness l of the acoustic beam, whereas $\delta\phi$ is the additional phase shift proportional to the sum $S_1 + S_2$ of longitudinal strain. In the present 2D or plane acoustic wave problem, with $S_3 = \partial u_3/\partial x_3 = 0$ for $\partial/\partial x_3 \equiv 0$, the sum of longitudinal strain $S_1 + S_2$ is nothing else but the *dilatation* or the relative change of material volume $\Delta = \delta V/V$.[11] The parameters of surface acoustic waves measured by the interferometric method thus find a physical significance as simple as the acoustic pressure associated with longitudinal waves in fluids.[15] In order to extract the dilatation Δ from the optical phase factor ϕ in Eq. (16), the component of the emerging light in the direction x_1 must be filtered. This component with an amplitude close to that of the incident light E_0 is then combined interferometrically with a reference light beam, as for pressure measurements in fluids.[15] As will be shown in Sec. IV A, the additional phase shift $\delta\phi(t)$ and consequently the acoustic dilatation $\Delta(t)$ associated with the guided wave can then be demodulated by a broadband electronic circuit to get a temporal linear response of low amplitude sinusoidal as well as short pulsed acoustic signals. Compared with the photoelastic technique, this interferometric measurement preserves not only the magnitude but also the phase information of acoustic waves.

In the particular case of pure shear waves with $S_1 = S_2 = 0$, the interferometric measurement becomes delicate, since the additional phase shift $\delta\phi$ of the light in Eq. (18) is zero. The acoustic information no longer appears in the phase shift, but in the magnitude of the light diffracted in the direction x_2 proportional to S_6, according to Eqs. (16) and (17). Nevertheless, by mixing the two components of the emerging light polarized in the directions x_1 and x_2 with the reference light, the shear strain S_6 has been detected linearly from the magnitude of the diffracted light.[16]

III. CHARACTERISTICS OF LAMB AND RAYLEIGH WAVES

In the preceding section, we have shown that the interferometric method can give access to the measurement of dilatation induced by guided acoustic waves. As examples, two typical guided waves were chosen to check the efficiency of this detection method: Lamb modes and Rayleigh waves propagating in an isotropic plate and substrate, respectively. The latter may be deduced, as shown below, from the former as a limit case when the plate becomes very thick. Before calculating the dilatation fields, it is instructive to briefly describe the principal characteristics of Lamb and the Rayleigh waves, especially the dispersion curves and the associated displacements.

A. Dispersion features for Lamb waves and the associated displacement fields

Lamb waves are modes guided inside an elastic plate with the stress-free boundary conditions.[19,20] The particle displacements are located in the sagittal plane formed by the direction of propagation and the axis normal to the plate plane. The particle displacement in an isotropic solid can be written in terms of potential functions:

$$\mathbf{u} = \nabla\Phi + \nabla\times\Psi. \tag{19}$$

Here $\Psi = (0,0,\Psi)$ is the rotational potential and Φ is the scalar potential, governed, respectively, by the following equations:

$$\nabla^2\Phi + k_L^2\Phi = 0, \quad \nabla^2\Psi + k_T^2\Psi = 0, \tag{20}$$

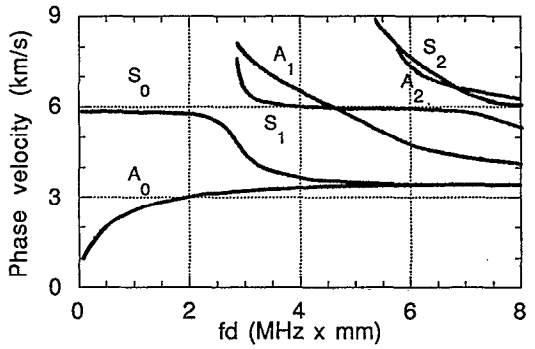

FIG. 3. Dispersion curves of Lamb waves in an isotropic plate of fused quartz.

where k_L and k_T are the wave numbers of longitudinal and shear plane waves. Applying the stress-free boundary conditions ($T_{22}=T_{12}=0$) at the two surfaces of the plate ($x_2=\pm d$), the characteristic (Rayleigh–Lamb) equations are obtained. It is found that, for a given value fd (frequency ×plate thickness), there exist, in general, multiple solutions for the phase velocity which satisfy the Rayleigh–Lamb equations. These correspond to the different Lamb wave modes. Figure 3 displays typical dispersion curves of the first few of these modes calculated for an isotropic plate (fused quartz). It is seen that the phase velocities depend upon the frequency for a given plate thickness: the modes are dispersive.

Lamb modes propagating in an elastic plate can be split up into two systems of symmetric (S) and antisymmetric (A) modes, respectively, according to the symmetry of particle displacements with respect to the middle plane of the plate. The symmetric modes have the u_1 component symmetric and the u_2 component antisymmetric with respect to the middle plane. These modes are thus longitudinal in nature. Conversely, the antisymmetric modes have u_2 symmetric and u_1 antisymmetric so that the plate motions for these modes are flexural. The following expressions for the displacement components u_1 and u_2 show the symmetry features of these modes:[19]

$$u_1=Ak_s\left(\frac{\cosh(q_sx_2)}{\sinh(q_sd/2)}-\frac{2q_ss_s}{k_s^2+s_s^2}\frac{\cosh(s_sx_2)}{\sinh(s_sd/2)}\right)\times\sin(k_sx_1-\omega t),$$
$$u_2=-Aq_s\left(\frac{\sinh(q_sx_2)}{\sinh(q_sd/2)}-\frac{2k_s^2}{k_s^2+s_s^2}\frac{\sinh(s_sx_2)}{\sinh(s_sd/2)}\right)\times\cos(k_sx_1-\omega t) \tag{21}$$

for symmetric modes and

$$u_1=Bk_a\left(\frac{\sinh(q_ax_2)}{\cosh(q_ad_z)}-\frac{2q_as_a}{k_a^2+s_a^2}\frac{\sinh(s_ax_2)}{\cosh(s_ad_2)}\right)\times\sin(k_ax_1-\omega t), \tag{22}$$

$$u_2=-Bq_a\left(\frac{\cosh(q_ax_2)}{\cosh(q_ad/2)}-\frac{2k_a^2}{k_a^2+s_a^2}\frac{\cosh(s_ax_2)}{\cosh(s_ad/2)}\right)\times\cos(k_ax_1-\omega t)$$

for antisymmetric modes. Here $q=\sqrt{(k^2-k_L^2)}$, $s=\sqrt{(k^2-k_T^2)}$, A and B are the arbitrary constants, and ks are the wave numbers of Lamb modes.

B. Dilatation fields of Lamb modes

Up until now, most of the observations performed on Lamb wave fields have been devoted to the individual components of displacement or stress.[19,20] Owing to the possibility offered by the interferometric method of directly measuring the dilatation (Sec. II B), we can now characterize the Lamb waves by the associated dilatation fields. Following Eq. (2), we write the dilatation in terms of the divergence of the displacement:

$$\Delta=S_1+S_2=\frac{\partial u_1}{\partial x_1}+\frac{\partial u_2}{\partial x_2}=\nabla\cdot\mathbf{u}. \tag{23}$$

Substituting Eqs. (21) and (22) into Eq. (23), respectively, yields the dilatation

$$\Delta_S=A(k_S^2-q_S^2)\frac{\cosh(q_Sx_2)}{\sinh(q_Sd/2)}\cos(k_Sx_1-\omega t) \tag{24}$$

for symmetric modes and

$$\Delta_A=B(k_A^2-q_A^2)\frac{\sinh(q_Ax_2)}{\cosh(q_Ad/2)}\cos(k_Ax_1-\omega t) \tag{25}$$

for antisymmetric modes.

The dilatations Δ have very simple forms when compared with the complete displacements. The field distributions across the plate are determined only by the parameter q related to the longitudinal acoustic wave, decoupled from the shear wave. As a matter of fact, substituting Eq. (19) into Eq. (23) yields

$$\Delta=\nabla\cdot\mathbf{u}=\nabla^2\Phi=-k_L^2\Phi, \tag{26}$$

where the relationship $\nabla\cdot(\nabla\times\Psi)=0$ has been taken into account. So the dilatation is proportional to the scalar potential Φ. Indeed, the dilatation can be deduced more simply from the scalar potential Φ rather than from the displacements.[19] Moreover, the symmetric and antisymmetric properties of Lamb modes are clearly demonstrated in Eqs. (24) and (25) by the hyperbolic sines and cosines. The dilatation fields provide, in addition to the displacements, an instructive and alternative vision on the Lamb wave motions.

Of particular interest in this work are the lowest symmetric S_0 and antisymmetric A_0 Lamb modes, which differ qualitatively from all other modes. It is seen in Fig. 3 that these modes exist for any value of the product fd, while the high-order modes have, for a given thickness, a cutoff frequency below which these modes cannot propagate. In the high-frequency or/and thick plate limit $fd\gg1$, the phase velocities of both modes S_0 and A_0 become asymptotic to the value of the Rayleigh wave velocity. Figure 4 presents the normalized dilatation fields of the fundamental Lamb modes

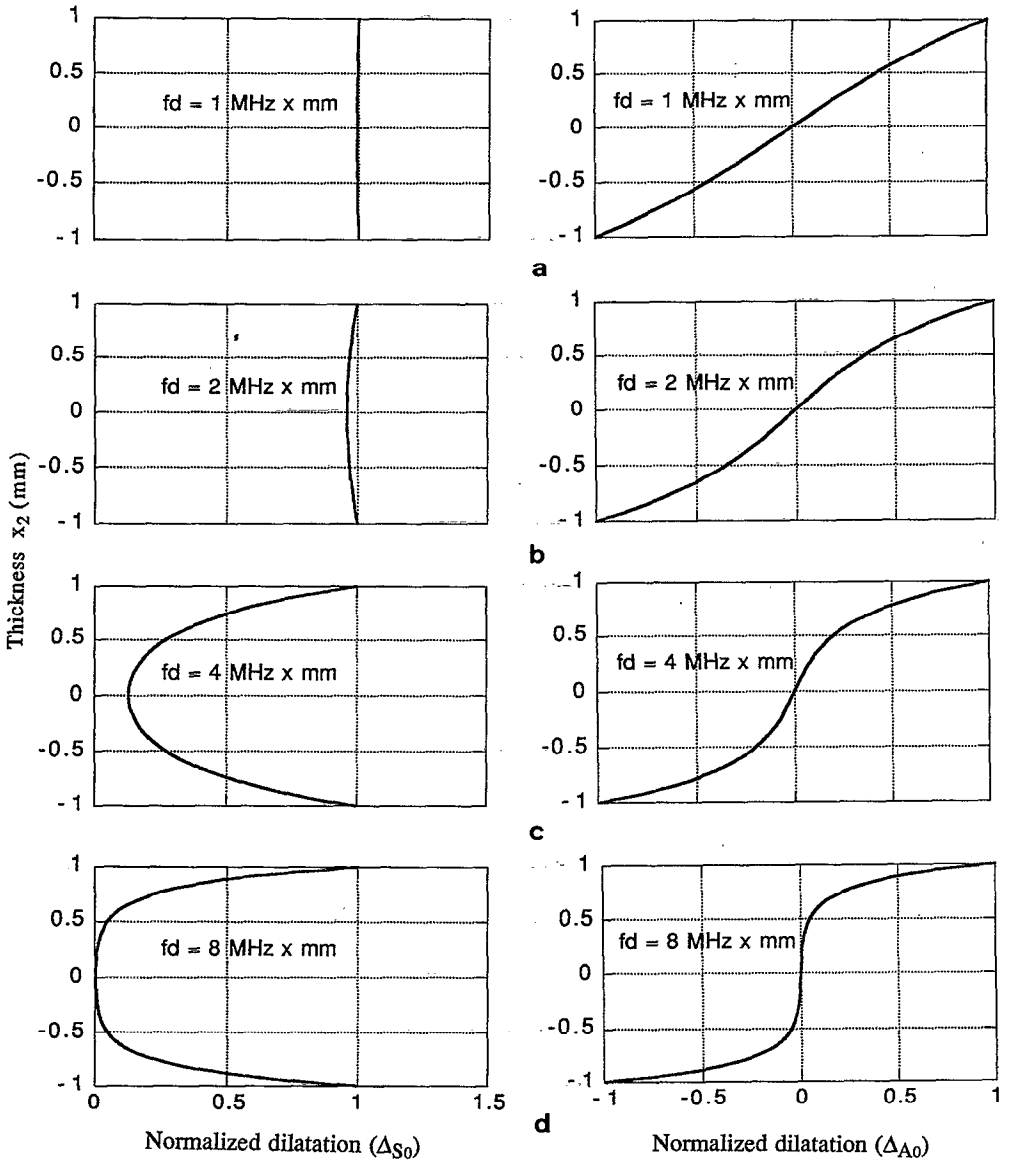

FIG. 4. Dilatation fields of the fundamental Lamb modes S_0 and A_0 calculated for different values of the product fd (frequency×thickness/2).

S_0 and A_0 across the plate as a function of the product fd. When $fd \leqslant 1$, the dilatation of the mode S_0 remains almost uniform across the plate [Fig. 4(a)], while the dilatation associated with the mode A_0 tends toward a linear function of x_2. The amplitude of dilatation for the mode A_0 reaches maximum at the boundaries of the plate ($x_2 = \pm d/2$) and decreases to zero at the middle plane [Fig. 4(a)]. When increasing the product fd, i.e., at high frequency or/and for a thick plate, the acoustic vibrations become more and more confined at the boundaries of the plate [Figs. 4(c) and 4(d)], approaching surface wave motion.

Figure 5 presents, respectively, the sum and the difference of the normalized dilatations associated with the modes S_0 and A_0 at $fd = 8$ MHz mm. Similar to particle displacements,[19–21] the dilatation combinations of the S_0 and A_0 modes construct, in the limit $fd \gg 1$, surface acoustic motions confined on the upper or lower boundaries of the plate. The dilatation field deduced directly from the Rayleigh wave

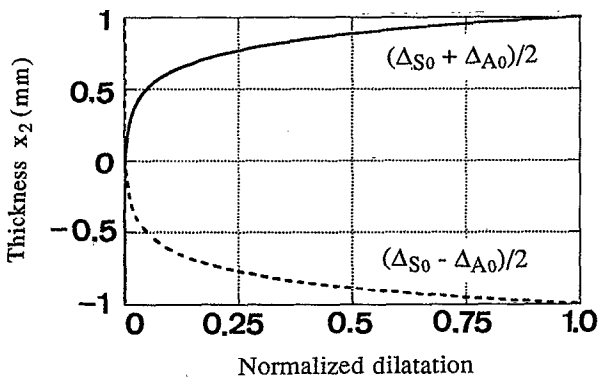

FIG. 5. Dilatation fields of surface waves on the upper and lower surfaces constructed from the sum or difference of equally normalized s_0 and a_0 modes for $fd \geqslant 8$ MHz mm.

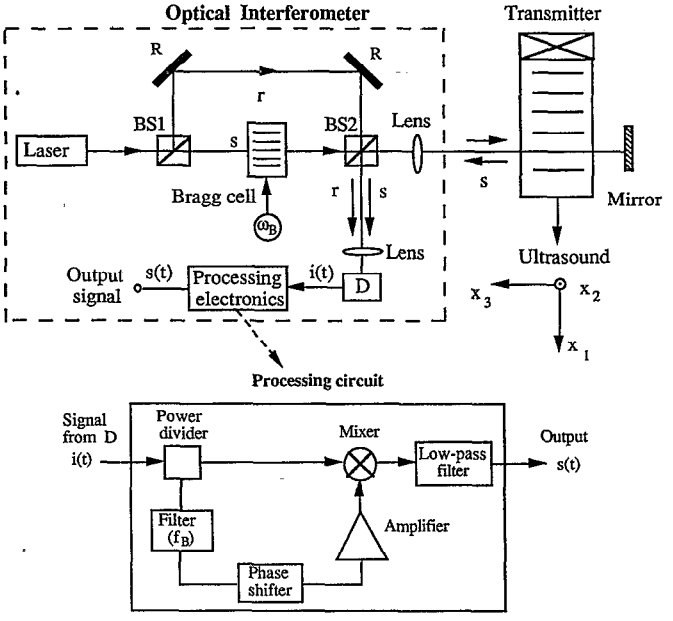

FIG. 6. Schematic diagram of the experimental arrangement.

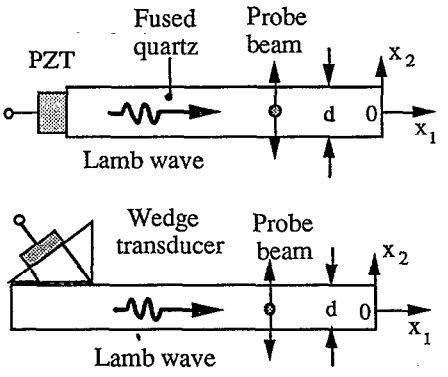

FIG. 7. Piezoelectric generation of the Lamb waves by a piezoelectric bar bonded (a) at the edge of the plate and (b) by a wedge transducer.

solution,[24] shown below, confirms these results:

$$\Delta_R=\Delta_0 \exp(-q_R x_2)\cos(k_R x_1-\omega t), \tag{27}$$

where Δ_0 is the amplitude of dilatation at the surface. The axis x_2 taken in Eq. (27) originates at the surface and is directed towards the medium. Unlike the displacement and stress fields,[19,20] the dilatation of the Rayleigh wave given by Eq. (27) decays as a single exponential inside the material. Such a monatomic decay picture, often used in reference books for illustrating surface wave motions,[20] therefore finds a physical support when dealing with the (scalar) dilatation field.

IV. EXPERIMENTS

A. Experimental setup

The schematic diagram of the experimental setup is shown in Fig. 6. A Mach–Zender type of interferometer[16,25] is used to measure the dilatations associated with the guided waves. The light coming from a laser is divided into two beams. The reference beam (r) goes directly to the photodiode, whereas the probe beam shifted in frequency by a Bragg cell (f_B=70 MHz) crosses twice normally the acoustic beam. Assume that the light coming from the laser source is expressed by $E_0 \exp i(2\pi f_L t)$, where E_0 is the amplitude and f_L is the frequency; the light fields of the reference beam and the probe beam interfering on the photodetector are as follows:

$$\begin{aligned} E_R&=E_0 \exp i(2\pi f_L t),\\ E_S&=E_0 \exp i[2\pi(f_L+f_B)t+2\delta\phi(t)], \end{aligned} \tag{28}$$

with $\delta\phi(t)$ the additional phase shift caused by the acoustic dilatation. The phase constants corresponding to the difference between the two optical paths are neglected here. Interference of the probe beam with the reference one results in a photocurrent

$$i(t)=I_0 \cos[2\pi f_B t+2\delta\phi(t)]. \tag{29}$$

Contrary to conventional Raman–Nath diffraction methods, the probe light beam in these experiments is made small compared to the acoustic wavelength, and the photodetector is placed in the optical near field to collect the total light beam before being diffracted into different orders. If the acoustic wavelength is comparable to the light beam, the resulted photocurrent $i(t)$ given in Eq. (29) should be averaged over the finite size of the light beam. More detailed discussion on this spatial filtering effect is given elsewhere.[26]

In order to extract the phase shift $\delta\phi(t)$ detected at a given position in the acoustic field, a broadband electronic processing used in acoustic displacement measurements[17,25] is adopted here. As shown at the bottom of Fig. 6, this processing consists in mixing the current signal $i(t)$ with a signal $I_0 \sin(2\pi f_B t)$, obtained by narrow-band filtering centered at f_B and phase shifting of the signal $i(t)$ by $\pi/2$. After passing through a low-pass filter in which high frequencies of the order of 2 f_B are eliminated, a signal $s(t)$ proportional to $\sin[\delta\phi(t)]\approx\delta\phi(t)$ (small acoustic signal approximation) is retained at the output of the interferometer. This signal is then calibrated to give quantitatively, according to Eq. (18), the dilatation wave form $\Delta(t)$ in sinusoidal as well as pulsed regimes. In this work, the detection bandwidth is 10 kHz–20 MHz and a sensitivity of 10^{-7} (for Δ)/mV is available in fused quartz.

Transparent solids used in our experiments are a plate ($60\times20\times2$ mm^3) and a block ($100\times30\times30$ mm^3) of fused quartz. Two piezoelectric methods were employed to generate the Lamb waves. In the first one, we bonded a piezoelectric bar at the end of the plate [Fig. 7(a)]. The dimensions of the bar are 15 mm in length, 1.8 mm in width, and 2 mm in thickness. If the bar is placed symmetrically with respect to the middle plane of the plate, the end of the plate is forced to vibrate uniformly in the length direction. This method is well suited for generating the symmetric mode S_0 at small values of fd, for which the mode S_0 is found to be predominately a longitudinal motion [Fig. 4(a), left]. The other method used a piezoelectric transducer and a water wedge deposited on the

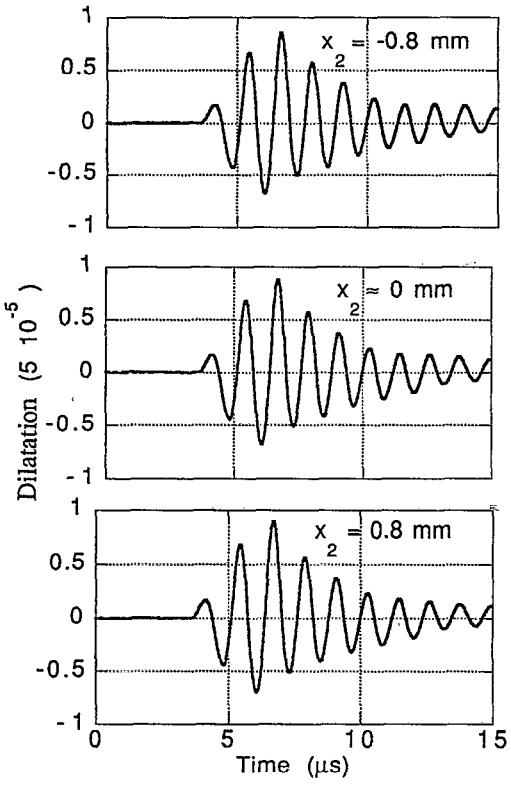

FIG. 8. Dilatation pulses of the Lamb mode S_0 in a 2 mm thick plate of fused quartz.

plate surface [Fig. 7(b)]. If the incidence angle of the plane wave in water is θ, Lamb waves will be generated according to $c=c_0/\sin\theta$. Here c is the phase velocity of Lamb waves and c_0 is the sound velocity in water. By varying the angle θ and the frequency of the incident acoustic wave, different Lamb modes can be generated according to the dispersion curves given in Fig. 3.[19] Taking into account the asymmetric configuration of the excitation, the wedge transducer is preferably used to generate the antisymmetric mode A_0 and the Rayleigh wave. The laser probe is placed about 2 cm away from the transducers. The probe beam is focused onto a spot of about 80 μm in diameter and moved along the thickness of the plate or block (Fig. 7).

B. Results and discussions

The dilatation pulses for the mode S_0 generated in a 2 mm thick plate are shown in Fig. 8. They are measured at $x_2=+0.4$, 0, -0.4 mm, respectively. The propagation velocity was measured as 5880 m/s close to the predicted value 5790 m/s (Fig. 3), for an actual value of $fd\approx 1.7$ MHz mm. It is seen that the amplitudes and the phases of the pulses remain almost unchanged across the plate, which agrees with the theoretical dilatation fields of the mode S_0 predicted for small fd (Fig. 4). Figure 9 presents the dilatation pulses of the mode A_0 measured at different depths $x_2=-0.8$, -0.4, 0, $+0.4$, $+0.8$ mm in the plate. As predicted by the calculation displayed in Fig. 4, the dilatation of the mode A_0 attains its maximum at the boundaries of the plate and changes sign from one side to the other, passing through a minimum at the middle of the plate. The comparison between the experimen-

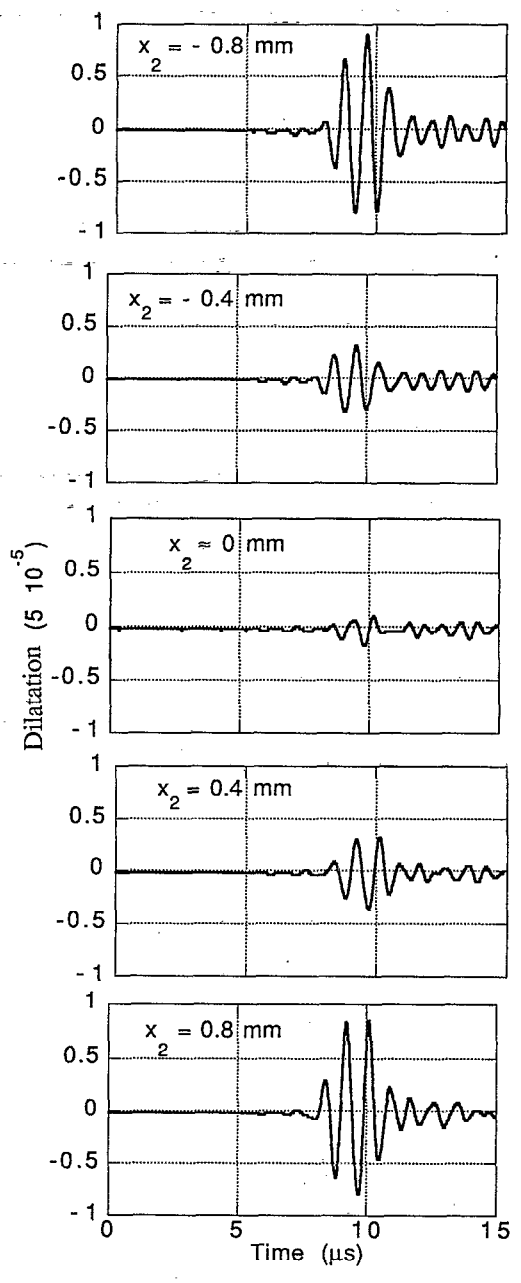

FIG. 9. Dilatation pulses of the Lamb mode A_0 in a fused quartz plate of 2 mm thickness.

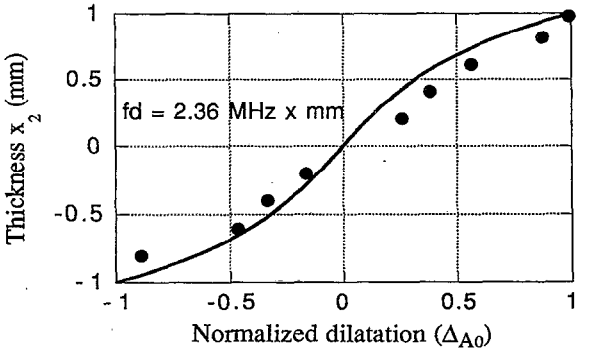

FIG. 10. Comparison between the dilatation of the mode a_0 calculated at $fd=2.36$ MHz mm and the experimental results.

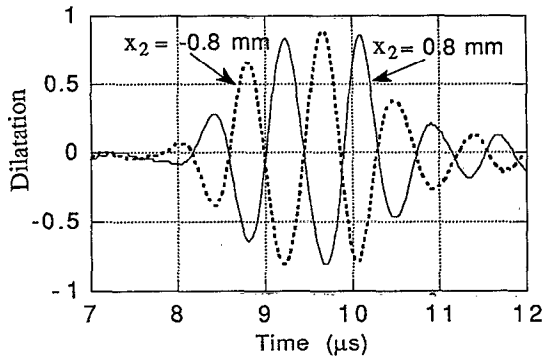

FIG. 11. π-phase change for the mode A_0 between the two measurements performed at $x_2=\pm 0.8$ mm.

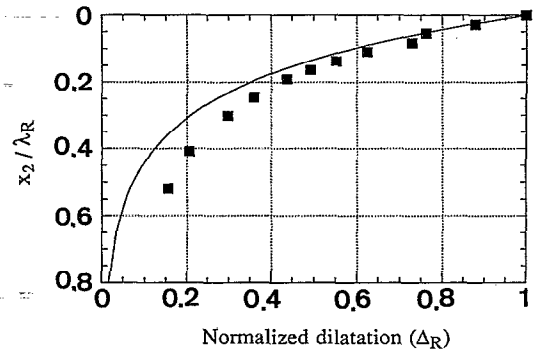

FIG. 13. Comparison between measured Rayleigh wave dilatations and theoretical prediction in terms of the ratio depth/wavelength.

tal results and the theoretical curve calculated at $fd=2.36$ MHz mm is shown in Fig. 10. The agreement is quite good. In Fig. 11 a π-phase change is clearly observed between the dilatation signals obtained at opposite sides of the middle plane ($x_2=\pm 0.8$ mm). This result clearly demonstrates the good phase sensitivity of the interferometric method. In previous experiments, the photoelastic technique[7] and the optical diffraction method[27–31] were also used to study the propagation of Lamb and Rayleigh waves. However, as mentioned in Sec. II A, the parameters measured by the photoelastic technique are physically not so simple and meaningful as those obtained by the interferometric method. In addition, the interferometric method is phase sensitive, which provides additional elements for characterizing wave propagation.

We now present measurements performed with a Rayleigh wave propagating on a block of fused quartz. A tone burst instead of a pulsed electric signal is used for wave excitation. The dilatation pulses of the Rayleigh wave are shown in Fig. 12. They are measured, respectively, at depths of 0.1 and 0.6 mm from the surface. For a central frequency of 1 MHz, the wavelength of the Rayleigh wave is about 3.4 mm. Figure 13 shows the decay of the Rayleigh wave dilatation in terms of the ratio depth/wavelength. The agreement between the theoretical curve and the experimental data is very satisfactory. The slight discrepancy investigated at large depths inside the substrate arises probably from the perturbation by leaky bulk waves coming from the wedge transducer.

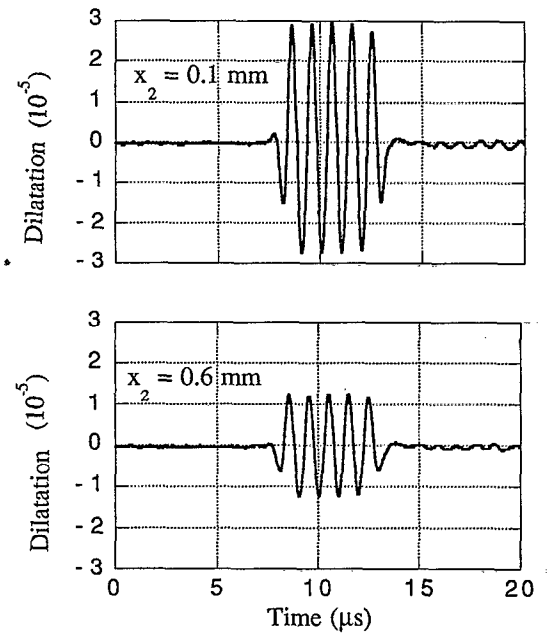

FIG. 12. Dilatation tone bursts of Rayleigh wave measured at 0.1 and 0.6 mm away from the surface of fused-quartz block.

V. CONCLUSION

We have presented an interferometric method for measuring surface acoustic waves inside a transparent solid. Starting from the refractive index ellipsoid perturbed by the acoustic strains, the principles of the photoelastic and interferometric measurements of acoustic waves were analyzed in a unified formalism. In contrast with the conventional photoelastic technique, the interferometric method is acoustic phase sensitive and gives access to the measurement of a meaningful physical parameter, i.e., the dilatation or the relative change in material volume. The Lamb modes S_0 and A_0 and the Rayleigh wave have been studied in detail in order to verify the present interferometric method. Compared to the displacement patterns, the dilatation field patterns of these waves are physically simple and instructive. The experiments performed in fused quartz are in agreement with theoretical predictions. We believe that, in addition to the full field visualization obtained with the photoelastic technique, the present interferometric method provides an interesting and alternative way to study guided acoustic waves. It may be helpful in nondestructive evaluation where the acoustic wave phase information is sometimes required.

ACKNOWLEDGMENTS

The authors wish to thank Professor B. Auld for the critical reading of the manuscript and very useful discussions about the subject.

[1] R. Lucas and P. Biquard, J. Phys. Paris **10**, 464 (1932).
[2] P. Debye and F. W. Sears, Proc. Natl. Acad. Sci. **18**, 409 (1932).
[3] J. Sapriel, *Acousto-optics* (Wiley, New York, 1979).
[4] A. Korpel, *Acousto-optics* (Marcel Dekker, New York, 1988).

[5] A. Yariv and P. Yeh, *Optical Waves in Crystals* (Wiley, New York, 1984).
[6] W. A. Riley, *IEEE Guide for Medical Ultrasound Field Parameter Measurement* (ANSI, New York, 1990), Chap. 4.
[7] C. F. Ying, *Physical Acoustics*, edited by R. N. Thurston (Academic, New York, 1990), Vol. 19, Chap. 7.
[8] F. D. Martin, L. Adler, and M. A. Breazeale, J. Appl. Phys. **43**, 1480 (1971).
[9] W. R. Klein and B. D. Cook, IEEE Trans. Sonics Ultrason. **SU-14**, 123 (1967).
[10] B. D. Cook, E. Cavanagh, and H. D. Dardy, IEEE Trans. Sonics Ultrason. **SU-27**, 202 (1980).
[11] G. S. Kino, *Acoustic Waves: Devices, Imaging, and Analog Signal Processing* (Prentice-Hall, Englewood Cliffs, NJ, 1987).
[12] A. C. Tam and W. P. Leung, Phys. Rev. Lett. **53**, 560 (1986).
[13] G. P. Davison and D. C. Emmony, J. Phys. E **13**, 92 (1980).
[14] *Photoacoustic and Photothermal Phenomena III*, edited by D. Bicanic, in Springer Series in Optical Sciences (Springer, Berlin, 1992), Vol. 69.
[15] X. Jia, G. Quentin, and M. Lassoued, IEEE Trans. Ultrason. Ferroelectr. Freq. Control **UFFC-40**, 67 (1993).
[16] X. Jia, A. Boumiz, and G. Quentin, Appl. Phys. Lett. **63**, 2192 (1993).
[17] J. P. Monchalin, IEEE Trans. Ultrason. Ferroelectr. Freq. Control **UFFC-33**, 485 (1986).
[18] C. B. Scruby and L. E. Drain, *Laser Ultrasonics—Techniques and Applications* (Hilger, New York, 1990).
[19] I. A. Viktorov, *Rayleigh and Lamb Waves* (Plenum, New York, 1967).
[20] B. A. Auld, *Acoustic Fields and Waves in Solids* (Wiley, New York, 1973), Vol. II, p. 89.
[21] G. W. Farnell, *Acoustic Surface Waves*, edited by A. A. Oliner (Springer, New York, 1978), Chap. 2.
[22] R. M. Montgomery and E. H. Young, Jr., J. Appl. Phys. **42**, 2585 (1971).
[23] S. V. Bogdanov and I. B. Yakovkin, Sov. Phys. Acoust. **18**, 104 (1972).
[24] Ch. Matteï, X. Jia, and G. Quentin, Acta Acustica **2**, 65 (1994).
[25] D. Royer and E. Dieulesaint, *Proceedings of 1986 Ultrasonics Symposium* (IEEE, New York, 1986), p. 527.
[26] X. Jia, L. Adler, and G. Quentin, *Proceedings of the 1994 Ultrasonics Symposium* (IEEE, New York, 1994), p. 833.
[27] P. Diodati, G. Tassi, and A. Allipi, Appl. Phys. Lett. **47**, 573 (1985).
[28] R. Magnusson and T. D. Black, J. Opt. Soc. Am. A **4**, 498 (1987).
[29] D. A. Larson, T. D. Black, M. Green, R. G. Torti, Y. J. Yang, and R. Magnusson, J. Opt. Soc. Am. A **7**, 1745 (1990).
[30] M. R. Chatterjee and S. T. Chen, J. Opt. Soc. Am. A **11**, 637 (1994).
[31] T. H. Chua and C. L. Chen, Appl. Opt. **28**, 3158 (1989).